Improving the Kinetics and Thermodynamics of Mg(BH4)2 for Hydrogen Storage

B. C. Wood, L. Klebanoff, V. Stavila, T. W. Heo, K. Ray, J. Lee, A. Baker, S. Kang, H. C. Yu, K. Thornton

November 13, 2017

Disclaimer

This document was prepared as an account of work sponsored by an agency of the United States government. Neither the United States government nor Lawrence Livermore National Security, LLC, nor any of their employees makes any warranty, expressed or implied, or assumes any legal liability or responsibility for the accuracy, completeness, or usefulness of any information, apparatus, product, or process disclosed, or represents that its use would not infringe privately owned rights. Reference herein to any specific commercial product, process, or service by trade name, trademark, manufacturer, or otherwise does not necessarily constitute or imply its endorsement, recommendation, or favoring by the United States government or Lawrence Livermore National Security, LLC. The views and opinions of authors expressed herein do not necessarily state or reflect those of the United States government or Lawrence Livermore National Security, LLC, and shall not be used for advertising or product endorsement purposes.

Final Report

(August 1, 2014 – September 30, 2017)

Project Title: Improving the Kinetics and Thermodynamics of Mg(BH$_4$)$_2$ for Hydrogen Storage

Project Period: August 1, 2014 – September 30, 2017
Date of Report: October 31, 2017

Recipient: Lawrence Livermore National Laboratory
Project # ST118

Project Director/Principal Investigator: Brandon Wood (Lawrence Livermore National Laboratory)
Subcontractors: Sandia National Laboratories, Livermore, CA; University of Michigan, Ann Arbor, MI

Team Members: Lennie Klebanoff (SNL), Vitalie Stavila (SNL), Tae Wook Heo (LLNL), Keith Ray (LLNL), Jonathan Lee (LLNL), Alex Baker (LLNL), ShinYoung Kang (LLNL), Hui-Chia Yu (U. Michigan), Katsuyo Thornton (U. Michigan)

Contact: Brandon Wood
Lawrence Livermore National Laboratory, 7000 East Avenue, L-413, Livermore, CA 94550
Phone: (925) 422-8391
Email: brandonwood@llnl.gov

Executive Summary

The objective of this project is to (1) combine theory, synthesis, and characterization across multiple scales to understand the intrinsic kinetic and thermodynamic limitations in MgB$_2$/Mg(BH$_4$)$_2$; (2) construct and apply a flexible, validated, multiscale theoretical framework for modeling (de)hydrogenation kinetics of the Mg-B-H system and related metal hydrides; and (3) devise strategies for improving kinetics and thermodynamics, particularly through nanostructuring and doping. The project has an emphasis on understanding and improving rehydrogenation of MgB$_2$, which has generally been less explored and is key to enabling practical use. The key accomplishments include:

- Computed and validated reference phase diagram of Mg-B-H including explicit thermal effects
- Demonstrated the role of microstructure, morphology, and particle size in determining the stability of reaction intermediates
- Developed new technique for size-selective synthesis of high-purity, unconfined MgB$_2$ nanoparticles and demonstrated 3x lower barriers for hydrogen dissociation and incorporation
- Showed that rate kinetics in the initial uptake regime of MgB$_2$ are connected to a multi-step process that is facilitated by interfaces and grain boundaries
- Showed that hydrogenation of MgB$_2$ can lead to the formation of BH$_4^{2-}$-like chemical species without persistent or long-lived intermediates
- Determined that rate limitations for deeper hydrogenation of MgB$_2$ are associated with B-B bond cleavage rather than H$_2$ dissociative adsorption
- Performed first full phase-field kinetics simulation of cycling between MgB$_{12}$H$_{12}$ and MgB$_2$, suggesting the possibility of different pathways for rehydrogenation and dehydrogenation in the hydrogen-poor domain

Results

Part 1: Thermodynamics

Motivated by the need to reconcile discrepancies between experiments and theoretical predictions from density functional theory (DFT) for the stability of reaction intermediates and pathways in the Mg-B-H system, a key goal of the project is the computation of more accurate thermodynamics of the bulk system. We evaluated three factors that are often neglected in DFT-computed reaction free energies: (1) explicit finite-temperature contributions to the free energy, including anharmonicity; (2) microstructural effects, including surface and interface contributions to the free energy; and (3) morphological factors such as amorphous phases, solid solutions, and polycrystallinity.

Validated reference phase diagram for Mg-B-H system

Complex borohydrides tend to exhibit highly anharmonic vibrational character associated with the rotation of B_xH_y molecular species. In conventional approaches based on the "quasiharmonic approximation", these vibrational contributions are approximated as stiff, harmonic modes, which can underpredict entropy. To address these finite-temperature free energy contributions, we applied a theoretical method developed jointly under this project and HyMARC. The method separates different contributions (diffusive, anharmonic, harmonic) from the vibrational density of states within long *ab initio* molecular dynamics simulations. Each contribution is fit to an appropriate analytical form, which allows more accurate computation of entropic contributions rather than extrapolating from zero-temperature results. As shown in Figure 1a, our calculations confirm that explicit calculations of the entropy can differ significantly from zero-temperature approximations, leading to mispredictions of the reaction conditions for (de)hydrogenation (we have used the predicted structures in Zhang *et al.* [1]). More importantly, these differences are not systematic—for instance, MgB_2 is well described by the harmonic approximation, whereas $Mg(BH_4)_2$ is not. It is likely that these effects will be augmented at surfaces where molecular reorientations are minimally constrained.

Our study also found that the enthalpies could be mispredicted by conventional DFT approaches within the generalized gradient approximation (GGE). As shown in Figure 1b, significant errors are implicit in DFT-computed formation enthalpies for gas-phase species when comparing to thermochemical reference data or high-level quantum chemical calculations. These same errors are likely to be propagated through the solid state reaction. However, Figure 1b demonstrates that these errors appear to depend on the number of B-H bonds in the anion molecular species. This implies that systematic correction may be possible. It is our hope that future studies will refine these corrections to provide more accurate computed enthalpies.

Using our revised entropy calculations and the DFT-GGA enthalpies, we computed free energies of the Mg-B-H compounds as a function of temperature (T) and H_2 partial pressure (pH_2), explicitly accounting for full finite-temperature dynamical contributions. These were used to construct a phase diagram for the conversion of $Mg(BH_4)_2$ to MgB_2 through the $MgB_{12}H_{12}$ solid-state intermediate, as shown in Figure 1c. In doing so, we use the experimental entropy for hydrogen gas, as is standard practice in *ab initio* thermodynamics. Although we also examined the possible formation of $Mg(B_3H_8)_2$, $Mg(B_{11}H_{14})_2$, and $MgB_{10}H_{10}$, none of these was predicted to be thermodynamically stable as an isolated phase, in agreement with the earlier calculations of Zhang *et al.* [1]. Stabilizing factors for these species are discussed further below.
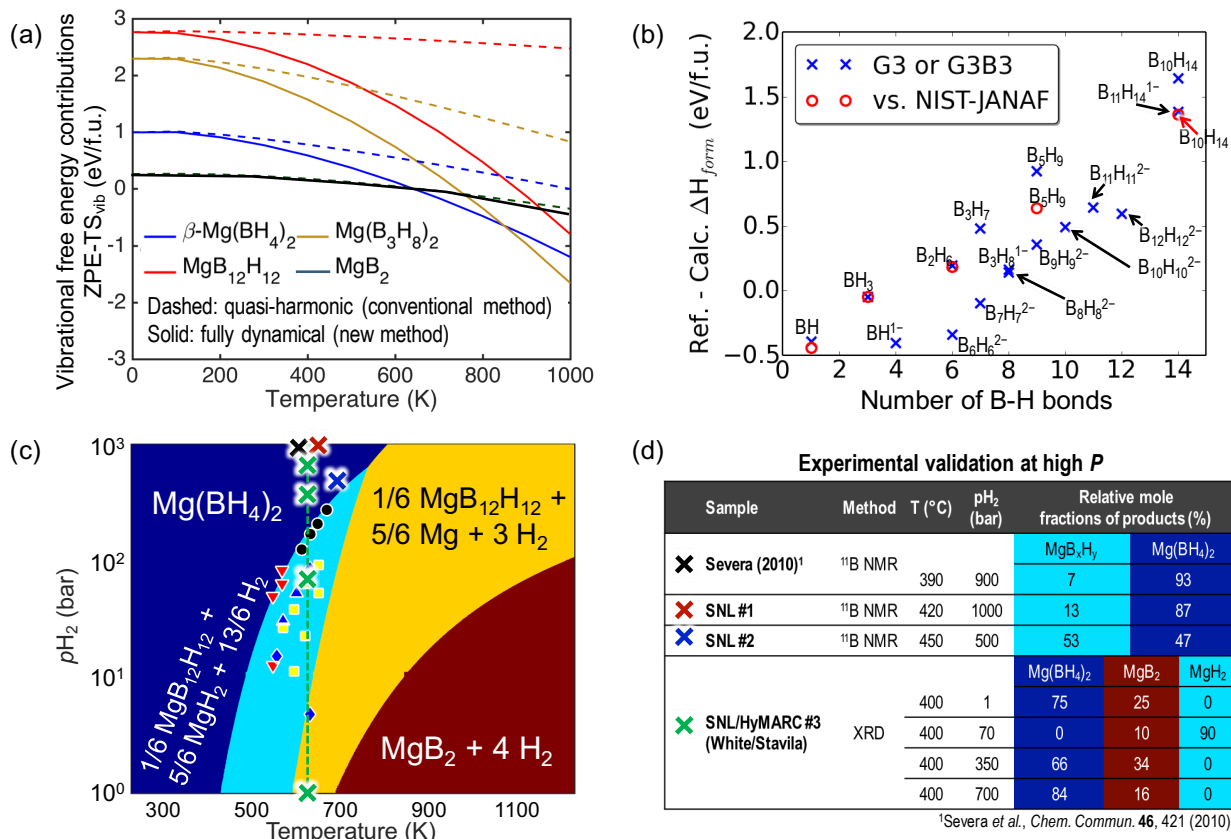
Figure 1. (a) Calculated thermal energy contributions from the conventional quasi-harmonic approximation (dashed lines) versus full dynamics including anharmonicity (solid lines) for $Mg(BH_4)_2$, MgB_2, $Mg(B_3H_8)_2$, and $MgB_{12}H_{12}$. (b) Comparison of computed formation enthalpies of B_xH_y intermediates with reference quantum chemical calculations (blue "x") and experimental thermochemical data (red circles). (c) Predicted Mg-B-H phase diagram. Experimental data for phase boundaries (from PCT) are shown for comparison: our unpublished data (black circles), Li *et al.* [2] (blue diamonds), Li *et al.* [3] (blue triangles), Yang *et al.* [4] (red downward triangles), and Han *et al.* [5] (yellow squares). At the points shown as "x", the relative phase fractions of $Mg(BH_4)_2$ and MgB_xH_y intermediates were also determined in order to benchmark the predictions. Experimental results at each of these points using ^{11}B NMR or XRD are summarized in (d), including previous measurements by Severa *et al.* [6].

We also calibrated the computed phase diagram in Figure 1c by shifting the temperatures to match the accurate phase boundary for the initial decomposition $Mg(BH_4)_2 \longleftrightarrow 1/6 \, MgB_{12}H_{12} + 5/6 \, MgH_2 + 13/6$ H_2 reaction derived from the experimental equilibrium plateau pressures. To maximize accuracy of this calibration, we also worked to obtain more precise PCT equilibrium data for dehydrogenation of $Mg(BH_4)_2$. In contrast to previous studies, which made measurements after only a couple of hours, we left the samples under fixed dehydrogenation conditions for days. The equilibrium plateau pressures extracted from our experiments (black circles) are shown alongside other published data in Figure 1c; a temperature shift of +230 K was required for the calibration. Note the spread in the available experimental data. In addition to our new PCT results, our data also agrees well with the measurements of Yang *et al.* [4]. Li *et al.* also observed Mg metal (at 360 °C, 4.8 bar) formed from decomposition of MgH_2 [2]. This point resides close to our phase boundary between $1/6 \, MgB_{12}H_{12} + 5/6 \, MgH_2 + 13/6 \, H_2$ and $1/6 \, MgB_{12}H_{12} + 5/6 \, Mg + 3 \, H_2$, as expected.

To further validate our computed phase diagram, we predicted the equilibrium phase fractions of the different compounds that should exist in the bulk system at different (pH_2, T) conditions. This was done by

performing a grand canonical minimization based on the free energies of the possible reactions, while considering the entropy associated with phase coexistence by approximating the system as an ideal mixture of phases. The predictions were compared with data obtained working through HyMARC at the high-pressure end of the phase diagram, where the phase behavior is predicted to have higher sensitivity and where less data is generally available. ^{11}B NMR and X-ray diffraction (XRD) were used to obtain additional data points for hydrogenated MgB_2 samples obtained through this project, as well as data published by Severa *et al*. [6]. These analyses were performed around 400 to 550 °C at various pressures up to 1000 bar. The phase fractions from NMR and XRD (the latter of which is unfortunately insensitive to the amorphous MgB_xH_y intermediates) are shown in Figure 1d for conditions corresponding to those in Figure 1c.

While NMR and XRD data include kinetic effects, our computed phase diagram is solely based on equilibrium thermodynamics. Nevertheless, the phase evolution trend found in NMR and XRD matched well with the trend in our predicted phase fractions, with higher levels of intermediates (or MgH_2 as a proxy for intermediates in XRD) appearing in regions near predicted phase boundaries. The predicted pressure at which MgB_xH_y intermediates become favored over $Mg(BH_4)_2$ generally agreed well with our calculations (not shown), with the equilibrium calculations showing a lower pressure threshold in accordance with expectations based on poor hydrogenation kinetics. The phase diagram in Figure 1c was used as a starting point to understand the effects of microstructure, nanosizing, and morphology on the phase stability and reaction pathway.

Predicted effects of morphology, microstructure, and particle size

The phase diagram in Figure 1c contains $MgB_{12}H_{12}$; however, it does not feature any other stable B_xH_y intermediates. Indeed, other tested phases based on these intermediates ($Mg(B_3H_8)_2$, $Mg(B_{11}H_{14})_2$, and $MgB_{10}H_{10}$) were not found to be stable with respect to $Mg(BH_4)_2$, MgH_2, MgB_2, and $MgB_{12}H_{12}$. This finding agrees with the previous computational results of Zhang *et al*. [1], upon which the tested crystal structures were based. Nevertheless, these species have been detected via NMR in numerous previous studies [6-7]. This suggests that they do not manifest as bulk crystalline phases. However, they may instead exist as dispersed molecular intermediates, clusters, interfacial species, or amorphous phases.

To explore these possibilities, we computed the formation energy associated with compounds formed via each of the abovementioned intermediates. The computations were done within three limits: first, the bulk "3-D" crystalline morphology; second, a "2-D" lattice of molecular species representing a possible surface or interfacial configuration; third, a "1-D" chain of molecular species that might also be present at a surface or interface; and fourth, a "0-D" isolated molecule. In each case, the mass-balancing MgH_2 or H_2 species were computed in the standard state. The results, shown in Figure 2a, demonstrate that $Mg(BH_4)_2$ and $MgB_{12}H_{12}$ are relatively stable in the bulk crystalline case compared to competing reactions, in agreement with Figure 1c. However, $Mg(BH_4)_2$ becomes far less stable when one considers the 0-D, 1-D, or 2-D configurations, in large part because the stability of the material derives from the bulk cohesive energy. In contrast, other species are far less sensitive to the morphology, showing very similar energetics for 0-D, 1-D, 2-D, and 3-D samples. In these cases, the stabilization derives primarily from the chemical bonds themselves. The results of Figure 2a strongly suggest that the other intermediate B_xH_y species are likely to manifest as dispersed molecular intermediates or at surfaces and interfaces rather than as bulk, condensed phases. This may explain why these intermediates are never found in crystalline form via XRD. It also suggests that the stability of the intermediates, as well as the reaction pathway, should be connected to the microstructure of the material. Thus, if the microstructure can be tuned, then it may be possible to alter the energy landscape. Note that the systems that show the smallest dependence on morphology (i.e., dimensionality) in Figure 2a are also the most likely to have poorest chemical kinetics, since their energy stabilization derives from the strong chemical bonding in the anion.

To further explore the potential importance of microstructure, we devised a computational method that goes beyond bulk thermodynamic methods used for the calculations in Figure 1 to also account for surface and interface energies in the computation of phase stability. These contributions should become more significant as the particle size decreases, since interfaces and surfaces will comprise a larger overall fraction of the volume. Rather than merely considering the lowest-energy surfaces, the effective surface energies of the different phases were computed by averaging over the low-index surfaces within a Wulff construction of the particle shape. Note that this is effectively an extension to the Grand Canonical Linear Programming (GCLP) method [8] that takes into account the microstructure and interfacial energies associated with multiphase coexistence. Unfortunately, detailed microstructural information for the Mg-B-H system was unavailable; we therefore instead tested our method on the $Li_3N/LiNH_2+2LiH$ complex metal hydride system, which exhibits many properties in common with $MgB_2/Mg(BH_4)_2$ but has few intermediates and a core-shell phase microstructure that can be readily assumed from available literature data (Figure 2b, top panels).
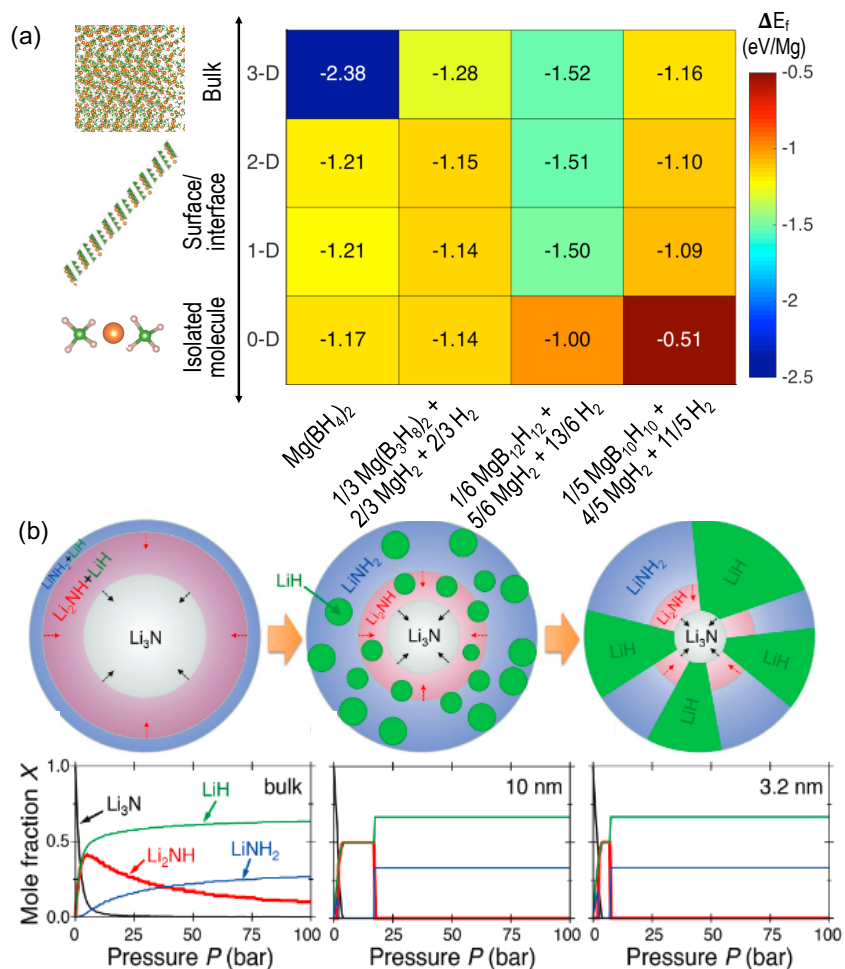

Figure 2. (a) Morphology-dependent stability of mass-balanced MgB_xH_y byproducts of $Mg(BH_4)_2$ decomposition based on computed formation energies of 3-D bulk crystals; 1-D and 2-D models representative of possible surface or interface geometries; and 0-D isolated molecules. (b) Schematic microstructure of hydrogenation from Li_3N to $LiNH_2 + 2 LiH$ (top panels) and predicted equilibrium mole fractions X of Li_3N, LiH, $LiNH_2$, and the Li_2NH intermediate as a function of H_2 pressure P upon isothermal hydrogenation. Results for the bulk material are compared with results for particles of diameter $d = 10$ nm and $d = 3.2$ nm, for which suppression of the Li_2NH intermediate is visible.

 As a validating case, we focused on predicting two peculiar behaviors associated with nanosizing that were found in extensive (de)hydrogenation data collected previously by our Sandia partners on the nanoconfined $Li_3N/LiNH_2+2LiH$ system: first, a transition from the low-pressure α-Li_3N phase to a high-pressure β-Li_3N phase; and second, a conversion from a two-step reaction to a single-step reaction that eliminates the otherwise stable Li_2NH intermediate, resulting in dramatically improved kinetics and reversibility. Our computational framework was able to properly predict the α-Li_3N/β-Li_3N phase stability reversal for particles smaller than 7.1 nm diameter, driven by a larger surface energy penalty for α-Li_3N.

On the other hand, the single-step reaction could be explained by considering surface energies alone. Accordingly, we devised an estimate for additionally accounting for the interface energies within the assumed phase microstructure. To do so, we relied on an empirical procedure for polygranular systems that estimates the interface energy as some fraction of the average surface energies of the constitutent phases [9]. Specifically, the DFT-computed surface energies σ_i and σ_j were used to compute the interfacial energy as $\gamma_{ij} = p\,(\sigma_i + \sigma_j)$, where p is a constant. Instead of fitting the constant p, we tested a range of values (from 0.3 to 0.7) to extract reasonable ranges of possible interfacial energies. Upon scanning across the space of possible p values, in all relevant cases our framework predicted near-complete elimination of the ordinarily stable Li_2NH intermediate once the size is reduced beyond ~5 nm (Figure 2b, bottom panels). This provided a concrete explanation for the experimentally observed single-step decomposition reaction. We emphasize that the disappearance of the intermediate results directly from the penalty associated with the formation of "nanointerfaces" *within* the particle, which become increasingly larger contributions as the particle size is reduced. Additional details can be found in Reference [10]. The possibility of using interfaces and phase microstructure to drive reaction pathways and kinetics is a compelling yet largely unexplored strategy for metal hydrides; we suggest it may be a viable research avenue for future studies.

Because microstructural information on the Mg-B-H system was unavailable, we did not apply the full nanointerface formalism used in Figure 2b to the system. However, some effects of particle size on the thermodynamic stability can be considered in an approximate way by considering the surface energies of each phase. To do so, we determined the Wulff construction for each phase, calculated an effective surface energy by averaging over the geometry of the Wulff construction, and then assumed a spherical geometry estimate the corresponding surface energy contribution. Note that this approximation treats each phase as an isolated particle rather than a realistic microstructure, meaning interfaces are considered as free surfaces. Nevertheless, the physical insights obtained are likely to transfer to the real system. Figure 3 shows the effect of particle size on the computed equilibrium phase diagram as a function of pressure upon hydrogenation (top panels) and dehydrogenation (bottom panels). The results suggest that smaller particles actually *increase* the thermodynamic driving force for the creation of the $MgB_{12}H_{12}$ intermediate, in large part because this phase has a very low surface energy. This should improve the thermodynamic driving force (and hence, the kinetics) of hydrogen uptake and release in the initial stages of the reaction; however, it should also create a problematic thermodynamic sink for continuing the reaction to completion.
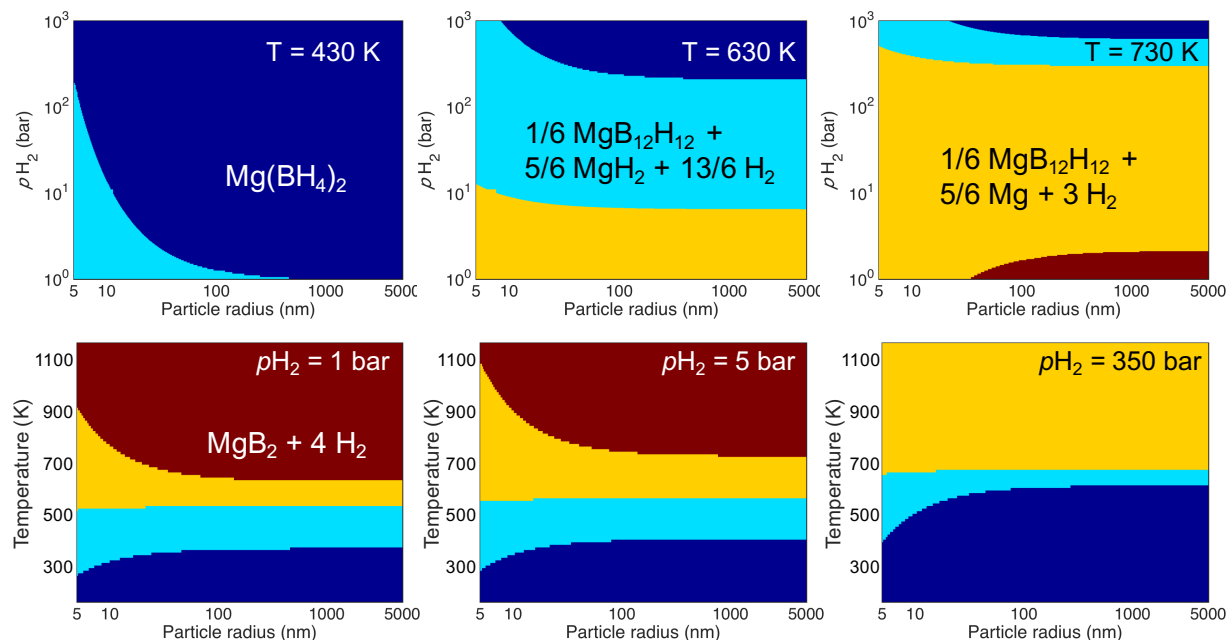
Figure 3. Predicted particle-size-dependent phase stability of Mg-B-H compounds for different temperatures (top panels) and hydrogen pressures (bottom panels).

Part 2: Synthesis and hydrogen uptake of nano-MgB$_2$ and MgB$_2$-additive mixtures

Synthesis and characterization of unconfined MgB$_2$ nanoparticles

The later phases of our project investigated pure and doped nanoparticles of MgB$_2$ that are freestanding without a confining medium. To test the effects of size and validate against our calculations and propposed mechanisms, we developed a new approach for the synthesis of phase-pure MgB$_2$ nanoparticles with narrow size distributions using surfactant-assisted ball-milling [11]. The basic approach involves ball milling commercial MgB$_2$ in an argon environment with a mixture of heptane, oleic acid and oleyl amine for ~ 20 hours, with the surfactant allowing the production of nanoparticulate MgB$_2$ free from agglomeration. Note that we used tungsten carbide (WC) milling hardware as stainless steel balls were previously found to introduce significant iron contamination. We found that tungsten carbide contamination could be minimized by interrupting the milling after 10 hours, removing and replacing the balls under the glove bag, and continuing to mill for another 10 hours. Measurements of hardware mass loss indicated that the total mass loss of WC during the 20 hours cumulative milling time could be kept to ~ 0.5 mole percent, which was deemed acceptable. Next, we performed centrifugal separation of the product taken up in heptane (at 5000 rpm for 25 minutes), with no supernatant observed. This material was washed 3 times with ethanol, consisting of adding ethanol to the deposit, ultrasonicating for 10 minutes, and centrifuging at 5000 rpm for 25 minutes with decanting of the ethanol/surfactant solution. The deposit was dried overnight, then taken up in heptane and driven through a 100 nm Teflon filter, leaving pure and size-selective MgB$_2$ nanoparticles. Transmission electron microscopy images confirmed that most of the particles we produced were < 50 nm in diameter with the size histogram indicating most of the particles are 10 to 20 nm in diameter.

We conducted a combination of Fourier transform infrared spectroscopy (FTIR) and X-ray absorption spectroscopy (XAS) to confirm the purity of the particles that is free of contamination from either the surfactants (oleic acid, oleyl amine), the solvent used in the nanoparticle dispersal (heptane) and

nanoparticle collection (ethanol), or oxidation. We used MgB_2 particles that passed through a 200 nm filter, and thus consists of particles less than 200 nm diameter. Figure 4a compares the FTIR of the MgB_2 nanoparticles with a spectrum from authentic B_2O_3, ethanol, oleic acide, and oleyl amine. There is no evidence for contamination in this material, at least to the sensitivity of FTIR which we estimate to be ~ 0.5 mole percent, and within the depth sensitivity (~ 3 μm). In addition, a test of possible contamination from air exposure at the ~ 50 nm depth level was performed by comparing the Mg K-edge XAS spectra of MgB_2 particles against those of MgO and Mg_3N_2 (Figure 4b). The results indicate the surfactant ball milled material looks very much like MgB_2, and not an oxidized or nitride sample, confirming the suitability of our sample handling procedures. Additional elemental analysis also supports the removal of oleyl amine (no N detected) and is also consistent with oleic acid removal (as little H was detected). Some residual ~ 5 mole % carbon contamination was observed of an initially unknown nature. The carbon K-edge XAS data indicates that the carbon exists primarily as WC not another form of carbon (e.g., graphitic carbon that can be suspected from degradation of heptane of the surfactants). More importantly, the residual carbon was unaffected by hydrogenating the MgB_2 sample at 140 bar H_2 and 365 °C for 120 hours, supporting the presence of the carbon as stable WC.

At the conclusion of MgB_2 nanoparticle synthesis, our synthesis procedures demonstrate the successful production of MgB_2 nanoparticles without significant contamination from the milling hardware, surfactants, or solvents. Using the new procedure, we found that from ball milling 19.8 grams of bulk MgB_2 in nine different 20 hours runs, we could cumulatively produce ~ 0.180 grams of MgB_2 nanoparticles, giving an overall yield of ~ 1% after the full procedure including surfactant removal and particle washing and drying.
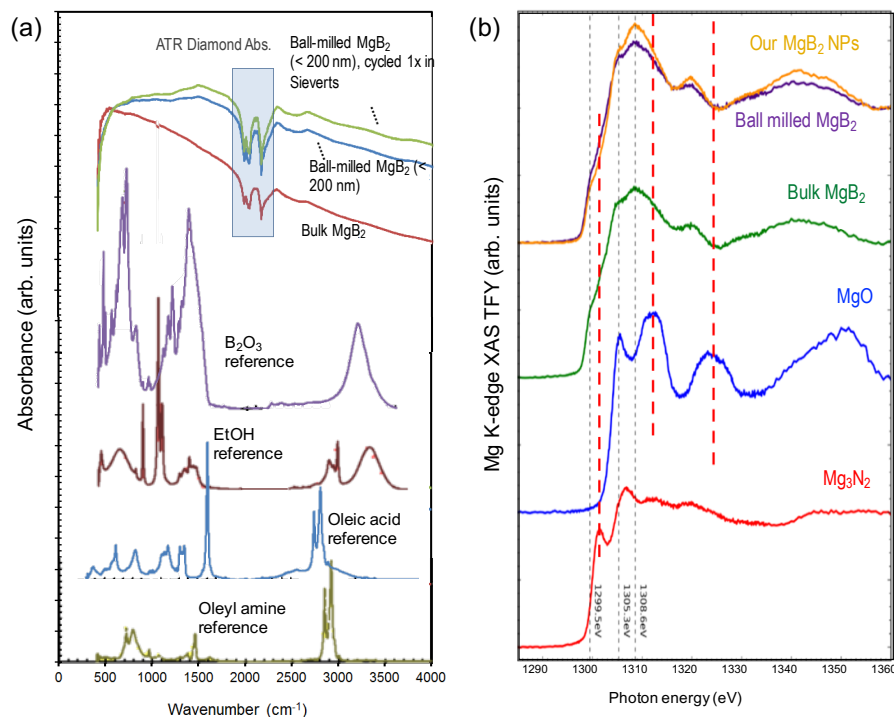

Figure 4. (a) FTIR spectra of our synthesized ball-milled nanoscale MgB_2 (< 200 nm diameter), compared with reference spectra for possible contaminants that might be introduced from solvents or exposure to air during the surfactant ball milling. (b) Mg K-edge XAS for our synthesized MgB_2 nanoparticles, compared with reference ball-milled and bulk samples and model oxides and nitrides. Both panels confirm synthesis of phase-pure MgB_2 particles.

Initial hydrogen uptake of bulk, nanoscale, and additive-modified MgB$_2$

Initial hydrogen uptake in bulk and nanoscale MgB$_2$ was assessed in a Sieverts apparatus, with results shown in Figure 5. The hydrogen uptake of bulk MgB$_2$ was compared with our unconfined nano-MgB$_2$ samples at 365 °C and 140 bar H$_2$ pressure. The improvement in uptake kinetics at early exposure for the nanoscale MgB$_2$ is immediately visible. (Note that the decrease in total sample wt.%H in the Sieverts data is likely due to the presence of residual surfactant, as these samples were extracted and tested prior to our refinement of the cleaning procedure described above.) Although these results clearly demonstrate the kinetic benefits of nanosizing, it should be emphasized that the Sieverts results can probe only the initial hydrogenation (< 1 wt.% H); the effect on the kinetics of the entire decomposition reaction has not yet been determined.

Besides the particle size, we commenced work on the nature of additives on the hydrogenation of MgB$_2$ (performed jointly with HyMARC). We prepared a mixture of 5 mole % TiF$_3$ or Pd in MgB$_2$ by ball milling together commercial MgB$_2$ and additives for two hours under argon. The initial hydrogenation of MgB$_2$/additive mixtures were performed at 140 bar H$_2$, up to ~ 1 wt. % H, with the results shown in Figure 5. The MgB$_2$/additive mixtures show the increased initial hydrogen uptake nano-MgB$_2$ by about a factor of 2 compared to the bulk MgB$_2$. As these accelerations similar to nano-MgB$_2$, it is not clear the improved kinetics is originated from the additives or as a result of ball milling the MgB$_2$, i.e., related to the microstructure. Additional studies to deconvolute the impact of additives from particle size effects will be undertaken in the context of HyMARC. Below we summarize our analysis of the kinetic mechanisms of initial hydrogenation in the context of bulk and nanoscale MgB$_2$.
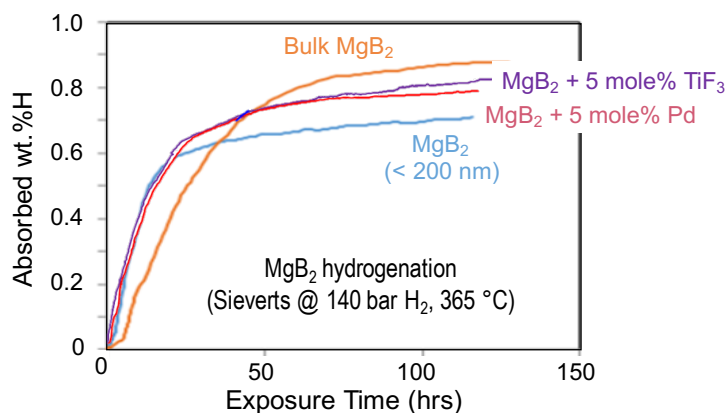

Figure 5. Sieverts hydrogen uptake data at 140 bar H$_2$ and 365 °C for bulk MgB$_2$, ball-milled MgB$_2$ nanoparticles (< 200 nm) and ball-milled MgB$_2$ particles with TiF$_3$ or Pd additives.

Part 3: Kinetics and mechanisms of hydrogen uptake in MgB$_2$

The kinetics studies in this project were broadly aligned along two aspects. The first aspect probed the chemical changes associated with the interaction of a material with hydrogen within the single-phase regime encountered at the initial stages of the reaction. Our approach for doing this involved combining *ab initio* chemical modeling, kinetic rate theory, spectroscopy, and isotope exchange experiments. The second aspect interrogated the structural phase transitions between different phases encountered at the later stages of the reaction. This relied on the development of a phase-field kinetic model parameterized

by the validated thermodynamic data in Part 1. Our focus was on the rehydrogenation of MgB_2, which has been comparatively less studied than the dehydrogenation process.

Analysis of products of initial hydrogenation of MgB_2

To understand the mechanism and kinetics of the initial stages of hydrogenation within the single-phase regime, we analyzed the bulk MgB_2 samples that were exposed to hydrogen within the Sieverts apparatus (Figure 5). The samples after hydrogen exposure exhibited a total uptake of ~0.85 wt.%H at 365 °C and 140 bar H_2 pressure prior to saturation, suggesting the sample remained in the single-phase regime. To understand how hydrogen is incorporated during initial hydrogenation, we performed synchrotron X-ray absorption spectroscopy (XAS), FTIR, and NMR analysis on the samples before and after hydrogen exposure, as shown in Figure 6. The FTIR spectrum for the initially hydrogenated sample (Figure 6a) showed features that were very consistent with $Mg(BH_4)_2$, without any additional features corresponding to $B_{12}H_{12}^{2-}$ or dispersed B-H bonds. In fact, the spectrum is a close match to a linear mixture of MgB_2- and $Mg(BH_4)_2$-like spectra. This implies that BH_4-like complexes are being generated even at relatively mild hydrogenation conditions. Other chemical intermediates are therefore not persistent at the timescales of the experiment, instead suggesting they transform rapidly to the hydrogen-rich product. From a molecular perspective, this implies that hydrogen is not atomically dispersed, but rather tends to cluster around a few B atoms to produce $Mg(BH_4)_2$-like molecular species. NMR studies also confirmed that BH_4^- was the dominant chemical product species. Note that no solid phase was found in XRD, confirming that the hydrogenation products remained in the low-concentration, pre-nucleation regime. We point out that previous work by Severa *et al.* found that conversion of MgB_2 to $Mg(BH_4)_2$ is possible at high pressures [6], and our thermodynamic phase diagram in Figure 1c confirms that this should be the preferred thermodynamic product. Nevertheless, our findings were unexpected at these mild conditions, suggesting that in this initial hydrogenation regime, the mechanism probably does not involve the formation of stable *closo*-borane intermediates, but rather is closely connected to the decomposition of the boron sheets in MgB_2.
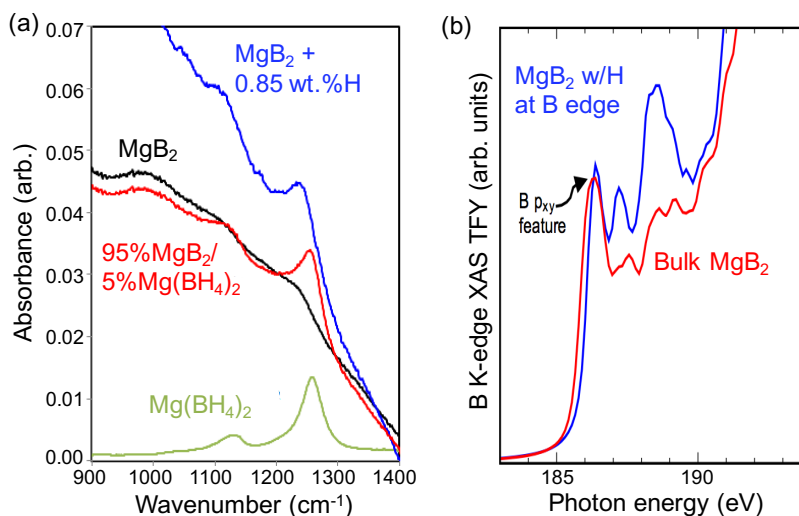

Figure 6. (a) FTIR spectrum of initially hydrogenated MgB_2 (0.85 wt.% H; blue), compared to reference spectra for $Mg(BH_4)_2$ (green) and MgB_2 (black). The blue spectrum is a close match to a linear $Mg(BH_4)_2/MgB_2$ mixture with the expected stoichiometric ratio (red). (b) Calculated XAS spectra at the B K-edge for hydrogen absorption at exposed B edge atoms in MgB_2 (blue), compared with the calculated spectrum for bulk MgB_2 (red). The blue spectrum agrees well with the experimental XAS spectrum (not shown), supporting our proposed mechanism of H bonding at boron edges. The signature boron p_{xy} feature (indicated with arrow), which is unique to MgB_2, is associated with the hexagonal boron sheets.

Further analysis of the initial hydrogenation product was performed with XAS. Comparison with reference XAS spectra showed that there is a signature in the boron K-edge XAS spectrum that is unique to MgB_2, whose disappearance can be tracked to indicate transitions to other chemical environments (marked as B p_{xy} in Figure 6b). In the experiments, this spectral signature, which is derived from the p_x and p_y states in the hexagonal boron sheets, was almost unaffected by the introduction of hydrogen (although there was some perturbation at somewhat higher photon energies). This suggests very few boron atoms exist in an altered chemical environment, implying the newly introduced hydrogen atoms concentrate at a small number of boron sites. To illustrate this point, consider that conversion to lower hydrogenation states in the form of $MgB_{12}H_{12}$ or homogeneously dispersed B-H bonds should theoretically result in a ~20% reduction in intensity of the key B p_{xy} spectral signature after 0.85 wt.%H uptake, contrary to the observations. In addition, comparison with single-phase reference spectra computed using DFT showed no signatures specific to intermediates (e.g., $MgB_{12}H_{12}$).

To better interpret the microscopic details of the MgB_2 hydrogenation process and rationalize the FTIR and XAS results, we performed a series of DFT calculations of the energetics, electronic structure, and XAS spectra of possible model interaction geometries (following the technique in Reference [12]). By directly comparing the computed and measured XAS spectra, we were able to judge which of the models are compatible with our experimental samples. The most intuitive structure involved atomic hydrogen incorporation into the bulk material via intercalation of H between Mg and B planes; however, this was very energetically unfavorable with respect to H_2 (binding energy of +0.74 eV per H atom), meaning there is no thermodynamic basis for such incorporation. Computing the XAS spectrum further allowed us to confirm that H incorporation into bulk MgB_2 is incommensurate with the experimental data, since even small amounts of hydrogen significantly impact the boron p_{xy} feature as hydrogen donates electrons into the boron sheets.

Since bulk intercalation of atomic hydrogen does not fit the data, we instead computed energetics of hydrogen insertion at edges and surfaces, which we used as simple models for solid-state interfaces. We find that these sites are significantly more favorable (binding energy of -0.59 to -0.93 eV per H atom for boron edges, and -0.5 eV per H atom for basal plane surfaces). These models were used to simulate an XAS spectrum, which showed excellent agreement with the experimental findings. The theoretical calculations for MgB_2 and MgB_2 with H at a B edge are shown in Figure 6b and demonstrate no significant change to the B p_{xy} energy or intensity (changes at higher photon energies are observed, as in the experiments). We conclude that H likely segregates to B edges occurs during initial hydrogenation. However, because exposed edges are very high in energy, it is more reasonable that high-energy strained bonds that lend themselves to facile B-B bond cleavage are the targets for hydrogen. These bonds should occur preferentially at interfaces and grain boundaries, and may act as magnets for subsequent hydrogen atoms to form highly coordinated BH_4-like complexes. We emphasize that although this mechanism may explain the initial stages of hydrogenation, the available binding sites for hydrogen are likely to become quickly saturated, which may explain the saturation behavior in the Sieverts uptake curves in Figure 5.

Kinetic mechanism of initial hydrogenation of MgB₂

Although the combined experiment-theory spectroscopic analysis justifies where hydrogen atoms are likely to bind, it does not explain the kinetics of this process, or how hydrogen is incorporated into the material. To answer these questions, we first applied a detailed kinetic analysis to the hydrogen uptake curves of bulk and nanoscale MgB_2 in Figure 5. Rather than extract an overall activation barrier for the reaction by fitting to kinetic equations, as is typically done, the Sieverts data were fitted using the Arrhenius equation to extract separate barriers for each level of hydrogenation (Figure 7a). The quality of the Arrhenius fits were also recorded as a measure of the heterogeneity of the process, since non-Arrhenius behavior is typical of such processes. Interestingly, we found that the barrier changes significantly during hydrogenation, even in the initial hydrogenation regime. As a result, there is no single rate-limiting process, but rather a variety of rate-limiting processes that become active at different stages of hydrogen uptake.

The initial uptake region (< 0.25 wt. % H) is non-Arrhenius, leading us to suspect that it represents the initial dissociation of H_2 at heterogeneous surface sites. For the bulk system, the corresponding estimated barrier is also quite similar to the dissociation barrier of 0.89 eV computed by Wang *et al*. [13]. From 0.2 to 0.7 wt. % H in the bulk material (0.3 to 0.4 wt.% H in the nanoscale material), the behavior is more regular, and likely indicates a diffusive and/or reactive regime. Finally, at later stages of the reaction, the barrier increases, indicating the onset of deeper hydrogenation and a new rate-limiting process. The barriers for all steps were found to be ~3x lower for the nanoscale material compared with the bulk material (even for this relatively large 200 nm particle size).
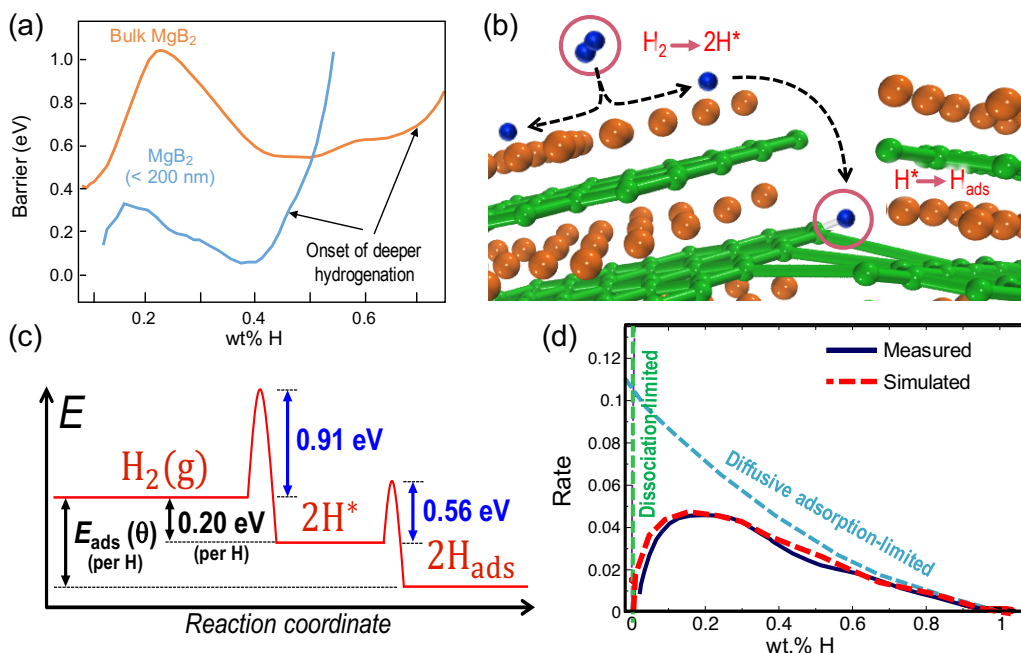

Figure 7. (a) Evolution of the effective kinetic barrier during initial hydrogenation of MgB_2, based on Arrhenius analysis of the Sieverts uptake curve in Figure 5 at different temperatures. (b) Proposed mechanism of initial hydrogenation of MgB_2, involving dissociation ($H_2 \rightarrow 2H^*$) and diffusive adsorption ($H^* \rightarrow H_{ads}$) to boron edge sites. (c) Energy diagram obtained by combining experimental and computational information used for our kinetic modeling. (d) Simulated uptake rate curves at 391 °C based on the energy landscape in (c), compared to experimental rate measurements under identical conditions. Results in the limit of a single-barrier rate limitations are also shown.

Focusing on the bulk material in the initial hydrogenation regime (ignoring the onset of deeper hydrogenation), we used our understanding to suggest a mechanism consisting of at least two steps. The first step was suggested to be dissociation on the basal-plane surface, and the second step was suggested to be surface diffusion from the dissociation sites and binding to edge sites (referred to collectively as "diffusive adsorption" hereafter). The proposed mechanism is depicted schematically in Figure 7b. To verify and systematically analyze this proposed mechanism, we devised a kinetic model that combines relevant non-equilibrium chemcial processes. We first constructed an energy diagram for the process, which is shown in Figure 7c. The energetics of the proposed intermediates and products (H_2 in the gas phase, dissociated surface H* atoms, and H_{ads} atoms bound to B edges) were first computed from simple DFT models. Next, the Arrhenius kinetic analysis of the experimental data in Figure 7a was used to paramterize the energy barriers of the corresponding chemical processes. The DFT calculations considered the coverage-dependent energy associated with binding hydrogen to exposed boron edge sites

(the sites compatible with the XAS and FTIR results), as well as the dissociation energy of H_2 on Mg-rich planes of $MgB_2(0001)$.

Using the constructed energy diagram, a simple reaction rate law, and a well established isotherm model, we derived a mathematical model of reaction equations for the successive dissociation/association and diffusive adsorption/desorption processes. Our model couples differential equations for each of these two processes as follows. The overall reaction may be written as $H_2\ (g) \leftrightarrow 2H^* \leftrightarrow 2H_{ads}$, where H* represents hydrogen at the initial dissociation site and H_{ads} represents hydrogen bound to the edges of hexagonal boron in MgB_2. The set of differential equations can be written as:

$$\frac{\partial c_{H^*}}{\partial t} = k_1 \cdot P_{H_2} - \tilde{k}_1 \cdot c_{H^*}^2 - \frac{\partial c_H^{ads}}{\partial t}$$

$$\frac{\partial c_H^{ads}}{\partial t} = k_2 \cdot c_{H^*}^2 \cdot c_s^3 \cdot (1-\theta)^2 - \tilde{k}_2 \cdot c_s^3 \cdot \theta^2$$

Here, c_{H^*}, c_H^{ads} are concentrations of H^*, H_{ads}, respectively, in *wt.% H*, P_{H_2} is the pressure of H_2 gas, and θ is the edge binding site (adsorption site) coverage by adsorbed hydrogen. Note that c_H^{ads} and θ are related by $c_H^{ads} = f_{cv}N_s\theta$, where $N_s\ (= N_s^0 \cdot \exp(-E^{acc}/k_BT))$ is the number of accessible edge binding sites participating in adsorption and f_{cv} is the unit conversion factor to *wt.% H*. We define $c_s = c_s^0 \exp(-E^{acc}/k_BT)$ as the *effective* concentration parameter of the accessible edge binding sites, where c_s^0 is the corresponding prefactor and E_{acc} is the associated activation energy. The kinetic coefficients k_1, $\tilde{k}_1$, k_2, and $\tilde{k}_2$ correspond to dissociation, association, adsorption, and desorption, respectively. These kinetic coefficients are expressed in the form $k_0\exp(-E/k_BT)$, where k_0 is the prefactor, E is the activation energy, and k_B is the Boltzmann constant, and T is the temperature. The prefactors k_0 were used as the only fitting parameters to calibrate the uptake timescales in the model against the experimental data.

The above equations are numerically solved simultaneously to capture the interactions between the two processes. Note that this model contains some elements that are computed (e.g., DFT-derived energetics for different coverages), some that are measured (e.g., experimentally derived activation energies), and some that are purely descriptive (e.g., prefactors for the kinetic rate constants fitted to match simulated and experimental uptake curves). Our kinetic model was able to capture the key behavior of the experimental uptake rates. Figure 7d shows the simulated isotherm uptake curve versus the experimentally measured result, from which it is clear that the two-step mechanism reproduces the major kinetic features of the experimentally observed uptake. For more detailed analysis, we conducted controlled simulations for a particular temperature ($T = 391$ ^{o}C) by manipulating the relative rates of the two operating reactions (dissociation/ association and diffusive adsorption). Simulated rate curves for reactions limited entirely by dissocation/association (green dashed line) and entirely by diffusive adsorption (blue dashed line) are shown in Figure 7d. As expected, the blue line exhibits a monotonous decreasing trend with the increasing extent of hydrogenation due to the site saturation. In addition, it converges to the later stage of the fully relaxed simulation and experimental result (represented by red curves in Figure 7d). Notably, this analysis confirms the presence of multiple governing processes, even in the initial hydrogenation regime, and strongly supports our proposed interpretation. The mechanism for initial hydrogenation of MgB_2 is discussed in detail in Reference [14].

Additional limitations for MgB₂ hydrogenation and the role of catalyst additives

The kinetic analysis discussed above focused on understanding the initial reaction of H_2 with MgB_2 prior to significant phase decomposition (up to ~1 wt.% H in our samples). In this regime, H-H bond breaking is only briefly rate limiting (< 0.3 wt.% H), followed by diffusive adsorption to form B-H bonds. However, the more significant rate limitations that inhibit the complete hydrogenation of MgB_2 under reasonable conditions occur upon subsequent hydrogenation. Unfortunately, the kinetic regimes associated with subsequent hydrogenation could not be directly accessed in the Sieverts apparatus.

Nevertheless, the onset of another significant rate limitation can be seen clearly at the highest Sieverts-accessible levels of hydrogenation in Figure 5; the likely origin of this kinetic barrier is discussed further below.

In speculating regarding the origin of key rate limitations for hydrogenation of MgB_2, it is important to note that our interpretation of the mechanism implies that H_2 dissociation should never be kinetically limiting beyond the very earliest stages of the reaction (~ 0.3 wt.% H according to Figure 7a). This implies that any overall rate enhancements in hydrogen uptake introduced by additives or nanosizing cannot be primarily due to faster H-H bond cleavage. Comparing hydrogen uptake and H_2 bond dissociation kinetics in bulk MgB_2, nanoscale MgB_2, and MgB_2 ball-milled with Pd and TiF_3 catalyst additives (Pd was chosen because it is known to catalyze gas-phase H_2 dissociation), the samples with additives show enhanced uptake with respect to the bulk material (Figure 5). However, these enhancements are very similar to nanoscale MgB_2, for which the likely origins of uptake enhancement were already discussed. If H_2 dissociation were significantly rate limiting over a broad range of compositions, then the catalyzed samples would be expected to show further enhancement.

Relative H_2 bond dissociation kinetics of the samples were also determined by examining if the materials in Figure 5 can readily form HD from mixtures of H_2 and D_2. The measurement consists of preparing known pressures of H_2 and D_2 (typically ~ 100 Torr) over the samples held at 200 °C, and measuring (with an RGA) the amount of HD produced. These measurements allow us to calculate the rate of the reaction $H_2 + D_2 = 2HD$, with $K = [HD]^2/[H_2]/[D_2]$, where the brackets indicate pressures. Under the chosen experimental conditions, the equilibrium rate constant should be $K_{eq} \sim 4.0$. As the HD exchange reaction was found slow in our samples, we measured the time to reach $K=1.5$ from 0 for each sample as an indicator of the relative efficiency of H_2 dissociation: 90 minutes for bulk MgB_2 versus less than one minute for MgB_2 + 5 mol. % Pd. HD exchange experiments for MgB_2 + 5 mol. % TiF_3 are in progress.

There are two observations to be made. First, the MgB_2 + 5 mol. % Pd sample has an H/D exchange rate over 90 times faster than bulk MgB_2, as expected given that Pd is an effective H_2 dissociation catalyst. Yet there is at most only a factor of two difference in their hydrogenation rates (Figure 5). Second, in an absolute sense, both samples have dissociated considerable amounts of H_2 after 90 minutes (1.5 hours), but in comparing 1.5 hours to the timescale of Figure 5, the hydrogenation still proceeds very slowly. Therefore, despite the significant amount of H-H bond breaking taking place on both samples, and especially a factor of 90 increase in the rate of H-H bond breaking presented by the MgB_2 + 5 mol. % Pd sample (Pd catalyzes H_2 dissociation, as expected), the hydrogenation kinetics are not strongly affected and remain comparatively sluggish. This confirms that H-H bond breaking is not significantly rate limiting for overall MgB_2 hydrogenation, as proposed.

It provides an important consideration for choosing additives, as one might has suspected that choosing an additive that promotes H-H bond breaking would be especially effective. Our study suggests this is not the case, and instead suggests that another mechanism is rate limiting. Our understanding is that the first steps of hydrogenation target accessible B atoms at defect sites (edges, grain boundaries, etc.). It is therefore likely that subsequent hydrogenation becomes limited by the availability of these sites. Once the defect sites are saturated, cleavage of ordinary B-B bonds and opening of B rings becomes necessary. Within this interpretation, further hydrogenation and the subsequent formation of molecular product phases require the generation of additional reactive boron sites by cleaving existing B-B bonds in MgB_2. This same bond cleavage is probably also critical for avoiding formation of (meta)stable *closo*-borates during hydrogenation. We therefore suggest that further efforts to destabilize MgB_2 should focus on additives or other approaches that facilitate the introduction of vacancies and defects in the hexagonal boron. This could be done via partial oxidation (e.g., solvents or additives), or possibly low-level aliovalent doping with non-hydride-forming species. Defects may also be introduced mechanically, which explains why MgB_2 uptake enhancements have been demonstrated under high-energy ball milling under

relatively reasonable conditions [15-16]. The effectiveness of future approaches for B-B bond cleavage and ring opening could be evaluated by monitoring the B K-edge XAS, which has key features that are sensitive to disruption of the aromatic π states.

Phase-field kinetic modeling of deeper hydrogenation of MgB$_2$

As an additional approach for probing the mechanisms of deeper hydrogenation of MgB$_2$ beyond the initial uptake regime, we developed a phase-field model informed by the DFT thermodynamic calculations described earlier in this report. These simulations provide a means to qualitatively understand the relationship between diffusion, phase formation, and reaction pathways as the reaction proceeds beyond the single-phase regime. Focusing on the hydrogen-poor region of the phase diagram (denoted Phase Triangle 3, the yellow region in Figures 8a and 8b), MgB$_{12}$H$_{12}$ and MgB$_2$. MgB$_{12}$H$_{12}$, MgB$_4$, MgB$_2$, and Mg were considered as possible stoichiometric compounds for the hydrogen-poor region of the phase diagram. These compounds were proposed as possible intermediates by Li *et al.* [3,17]. The underlying free energy landscape was constructed based on our DFT-computed free energies at 350 °C, with intermediate compositions interpolated using a mathematical smoothing function. Note that this is the first demonstration of a phase-field model for understanding kinetics in complex hydrides.

Multiphase phase field simulations [18-19] were performed to examine the reaction pathways for rehydrogenation of MgB$_2$. In the simulations, a boundary condition corresponding to a high H chemical potential (i.e., high H$_2$ pressure) outside the particle is imposed to trigger the initial rehydrogenation. This allows the large nucleation barrier associated with the initial insertion of H into MgB$_2$ to be overcome. Note that this barrier is associated with the steep gradient of the energy landscape near MgB$_2$ and suggests additives are necessary to catalyze B-B bond cleavage, as has been proposed. Figure 8a shows rehydrogenation simulation results if B and Mg mobilities are assumed to be sluggish compared to H mobility. As H is inserted into the particle, a core-shell morphology forms with a non-stoichiometric shell (the composition of which is approximately MgB$_4$H$_4$) and a core of MgB$_2$. The reaction pathway follows the pathway indicated in the left panel of Figure 8a: the low B and Mg mobilities hinder separation between these two species to form stoichiometric compounds and metallic Mg.

Another simulation was performed to examine the case when B and Mg mobilities are higher than H mobility (Figure 8b). Although this condition is unrealistic for bulk MgB$_2$, it represents a case for which B-B bond cleavage and Mg extraction are catalyzed. The result shows a very different morphological evolution from the previous one. As shown in Figure 8b, a MgB$_{12}$H$_{12}$ layer forms near the particle surface as H is inserted into the particle. As rehydrogenation proceeds, phases with high Mg concentration emerge from the MgB$_2$ region. Next, MgB$_4$ phases form and grow from the MgB$_2$ region. Meanwhile, the MgB$_4$ phases transform to MgB$_{12}$H$_{12}$, which grows with Mg inclusions. This composition evolution is indicated in the left panel of Figure 8b. The overall kinetics of hydrogen uptake from the two rehydrogenation simulations in Figures 8a and 8b are shown in Figure 8c. It is clear that faster mass transport of Mg and B (as in Figure 8b) improves reaction kinetics, presumably because the composition evolution is allowed to occur via the low-energy pathways, i.e., from MgB$_2$ via MgB$_4$ to MgB$_{12}$H$_{12}$. Note that in the case of MgB$_2$, mass transport of B is closely related to B-B bond cleavage, which should be rate limiting in deeper stages of hydrogenation, as discussed above. Overall, the results in Figure 8 point to a close coupling between microstructure evolution, phase pathway, and (de)hydrogenation kinetics that merits further exploration.
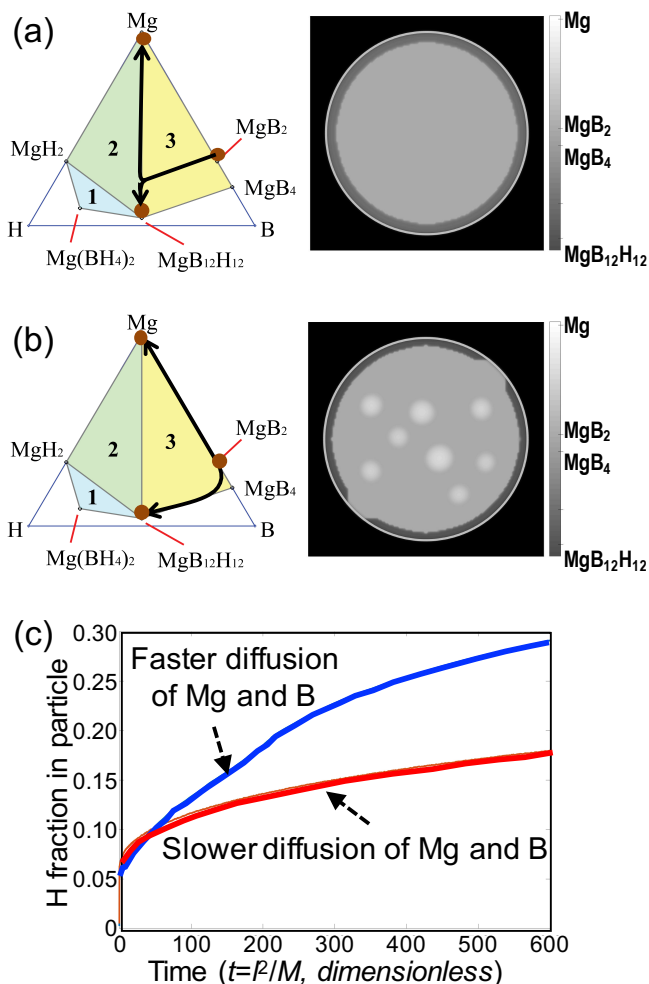
Figure 8. Simulated kinetic pathways and microstructure evolution during rehydrogenation of MgB_2 in the case where (a) B and Mg mobilities are two orders of magnitude slower than H mobility, and (b) B and Mg mobilities are two orders of magnitude faster than H mobility. (c) Comparison of overall hydrogen uptake kinetics for the cases described in (b) and (b). T

Conclusions and outlook

Although MgB_2 uptake was not improved to a viable threshold for fast hydrogen storage, our study succeeded in elucidating many of the key mechanisms involved in the hydrogenation of the material. These insights will be extremely valuable for directing future research efforts towards improving hydrogenation kinetics. The key conclusions and implications are listed below.

- Unconfined MgB_2 nanoparticles can be synthesized with high purity and size selectivity using a surfactant-assisted ball milling approach.
- *Ab initio* molecular dynamics calculations show that anharmonic molecular rotations play a significant role in determining entropically driven phase stability. Among other factors, these may depend on density, which could be reduced via additives, microstructural engineering, or interfacial strain.
- After correcting for anharmonic effects and calibrating the computations against PCT data, $MgB_{12}H_{12}$ is found to be the only thermodynamically preferred MgB_xH_y condensed phase intermediate.

- MgB_2 and $Mg(BH_4)_2$ have a strong tendency to form crystalline phases, whereas DFT calculations indicate that most intermediates can form molecules, amorphous phases, or interfacial segregates without significant enthalpy penalty. This explains the presence of experimentally observed non-crystalline MgB_xH_y intermediates. A possible strategy for eliminating these intermediates is to introduce chemical additives that may alter the relative stability of molecular vs. condensed phases.
- Within the initial hydrogenation regime, it is possible to create molecular $Mg(BH_4)_2$ from MgB_2 at relatively mild conditions without persistent intermediates. Using a combined experiment-theory approach, the mechanism for H_2 incorporation was shown to involve at least two steps: dissociation and diffusive adsorption at high-energy boron edge sites.
- To aid further hydrogenation, additional boron sites must be generated by cleaving existing B-B bonds in MgB_2. Such cleavage likely becomes the first significant rate limitation in the formation of molecular product phases once high-energy boron edge sites are saturated (> 1 wt.% H in our samples), and may also be critical for avoiding formation of (meta)stable *closo*-borates. This hypothesis is supported by isotopic exchange experiments.
- The mechanism of MgB_2 decomposition suggests that creating additional reaction sites via vacancies, edges, and grain boundaries should aid uptake kinetics. Strategies for doing so could include ball milling, nanosizing, cation substitution, or solvents/additives that may alter B-B bonding in MgB_2.
- Calculations show that nanosizing is unlikely to help the thermodynamics for full interconversion of MgB_2 and $Mg(BH_4)_2$. However, unconfined MgB_2 nanoparticles exhibit 3x lower activation energy barriers for initial H_2 uptake. Similar results were obtained for MgB_2 when ball milled with known catalysts. This can be understood by considering at least two factors: the thermodynamic driving force for decomposition of MgB_2 to MgB_xH_y intermediates increases; and nanosizing or ball milling introduces additional boron reaction sites for interaction with H_2.
- Internal microstructure can affect reaction pathways and intermediate stability in nanoparticles. This occurs because energy penalties associated with the formation of internal interfaces becomes increasingly large as particle size decreases. This factor was shown to be relevant for the Li-N-H system, and may likewise play a role in the Mg-B-H system. Further study of the Mg-B-H microstructure will be required for full assessment of this possibility.
- The first phase-field simulation of hydrogen uptake in complex hydrides was demonstrated for MgB_2. The results evidenced a strong connection between diffusion rates, reaction pathways, and microstructure evolution for hydrogenation of MgB_2.

Publications/Presentations

1. Wood, B.C., V. Stavila, N. Poonyayant, T.W. Heo, K.G. Ray, L.E. Klebanoff, T.J. Udovic, J.R.I. Lee, N. Angboonpong, and P. Pakawatpanurut. "Nanointerface-driven reversible hydrogen storage in the nanoconfined Li-N-H system." *Adv. Mater. Interfaces* 4 (2017): 1600803.
2. Ray, K.G., L.E. Klebanoff, J.R.I. Lee, V. Stavila, S. Kang, T.W. Heo, M. Bagge-Hansen, J. White, P. Shea, Y.-S. Liu, and B.C. Wood. "Elucidating the mechanisms of MgB_2 initial hydrogenation via a combined experiment-theory study." *Phys. Chem. Chem. Phys.* 19 (2017): 22646.
3. Stavila, V., N. Poonyayant, T.-W. Heo, K. Ray, T.J. Udovic, N. Angboonpong, P. Pakawatpanurut, L.E. Klebanoff, B.C. Wood. "Nanostructuring: A Route for Enhancing Reversibility in Metal Hydrides?" *Gordon Conference on Hydrogen-Metal Systems*, Easton, MA, July 2015.
4. Stavila, V. *et al*. "Understanding and controlling hydrogen release and uptake in complex metal hydrides." *Pacifichem*, Honolulu, HI, December 2015.

5. Wood, B.C. *et al*. "Nanointerface-driven reversible hydrogen storage in the nanoconfined Li-N-H system." *Materials Research Society Spring Meeting*, Phoenix, AZ, April 2016.

6. Ray, K.G. *et al*. "X-ray absorption and emission spectroscopy of the initial hydrogenation of MgB_2," *Advanced Light Source User Meeting*, Berkeley, CA, October 2016 [invited].

7. Kang, S. *et al*. "Beyond-ideal modeling of (de)hydrogenation in complex metal hydrides," *International Symposium on Hydrogen Energy*, Waikoloa, HI, February 2017 [invited].

8. Kang, S. *et al*. "Thermodynamics and Kinetics at Interfaces of Metal Hydrides for Hydrogen Storage." *American Chemical Society Meeting*, San Francisco, CA, March 2017.

9. Wood, B.C. "Complex dynamics in metal borohydrides: From hydrogen storage to solid-state batteries." *Hydrogen Metal Systems Gordon Research Conference*, Easton, MA, July 2017 [invited].

10. Wood, B.C. *et al*. "Improving the kinetics and thermodynamics of $Mg(BH_4)_2$ for hydrogen storage." *U.S. DOE Hydrogen and Fuel Cells Program Annual Merit Review*, Washington, D.C., June 2015.

11. Wood, B.C. *et al*. "Improving the kinetics and thermodynamics of $Mg(BH_4)_2$ for hydrogen storage." *U.S. DOE Hydrogen and Fuel Cells Program Annual Merit Review*, Washington, D.C., June 2016.

12. Wood, B.C. *et al*. "Improving the kinetics and thermodynamics of $Mg(BH_4)_2$ for hydrogen storage." *U.S. DOE Hydrogen and Fuel Cells Program Annual Merit Review*, Washington, D.C., June 2017.

References

1. Zhang, Y., E. Majzoub, V. Ozoliņš, and C. Wolverton. "Theoretical Prediction of Metastable Intermediates in the Decomposition of $Mg(BH_4)_2$." *J. Phys. Chem. C* 116 (2012): 10522-10528.

2. Li, H.-W., K. Miwa, N. Ohba, T. Fujita, T. Sato, Y. Yan, S. Towata, M. W. Chen, and S. Orimo. "Formation of an intermediate compound with a $B_{12}H_{12}$ cluster: Experimental and theoretical studies on magnesium borohydride $Mg(BH_4)_2$." *Nanotechnology* 20 (2009): 204013.

3. Li, H-W., K. Kikuchi, Y. Nakamori, N. Ohba, K. Miwa, S. Towata, and S. Orimo. "Dehydriding and rehydriding processes of well-crystallized $Mg(BH_4)_2$ accompanying with formation of intermediate compounds." *Acta Materialia* 56 (2008): 1342-1347.

4. Yang, J., X. Zhang, J. Zheng, P. Song, and X. Li. "Decomposition pathway of $Mg(BH_4)_2$ under pressure: Metastable phases and thermodynamic parameters." *Scripta Materialia* 64 (2011): 225-228.

5. Han, Jeong Seb, and Sun Jung Kim. "A Study of the Pressure-Composition-Temperature Curve of $Mg(BH_4)_2$ by Sieverts Type Apparatus." *Korean J. Met. Mater.* 53 (2015): 815-819.

6. Severa, G., E. Rönnebro, and C.M. Jensen. "Direct hydrogenation of magnesium boride to magnesium borohydride: Demonstration of > 11 weight percent reversible hydrogen storage." *Chem. Commun.* 46 (2010): 421-423.

7. Chong, M., A. Karkamkar, T. Autrey, S. Orimo, S. Jalisatgi, and C.M. Jensen. "Reversible dehydrogenation of magnesium borohydride to magnesium triborane in the solid state under moderate conditions." *Chem. Commun.* 47 (2011): 1330-1332.

8. Ozoliņš, V., A.R. Akbarzadeh, H. Gunaydin, K. Michel, C. Wolverton, and E.H. Majzoub. "First-principles computational discovery of materials for hydrogen storage." *J. Phys. Conf. Ser.* 180 (2009): 012076.

9. Porter, D.A., and K.E. Easterling. *Phase Transformations in Metals and Alloys*. 2nd ed.; Chapman & Hall: London, UK (1992).

10. Wood, B.C., V. Stavila, N. Poonyayant, T.W. Heo, K.G. Ray, L.E. Klebanoff, T.J. Udovic, J.R.I. Lee, N. Angboonpong, and P. Pakawatpanurut. "Nanointerface-driven reversible hydrogen storage in the nanoconfined Li-N-H system." *Adv. Mater. Interfaces* 4 (2017): 1600803.

11. Poudyal, N., C.-B. Rong, and J.P. Liu. "Morphological and magnetic characterization of Fe, Co, and FeCo nanoplates and nanoparticles prepared by surfactants-assisted ball milling." *J. Appl. Phys.* 109 (2011): 07B526.

12. Prendergast, D., and G. Galli. "X-ray absorption spectra of water from first principles calculations." *Phys. Rev. Lett.* 96 (2006): 215502.

13. Wang, Y., K. Michel, Y. Zhang, and C. Wolverton. "Thermodynamic stability of transition metals on the Mg-terminated $MgB_2(0001)$ surface and their effects on hydrogen dissociation and diffusion." *Phys. Rev. B* 91 (2015): 155431.

14. Ray, K.G., L.E. Klebanoff, J.R.I. Lee, V. Stavila, S. Kang, T.W. Heo, M. Bagge-Hansen, J. White, P. Shea, Y.-S. Liu, and B.C. Wood. "Elucidating the mechanisms of MgB_2 initial hydrogenation via a combined experiment-theory study." *Phys. Chem. Chem. Phys*. 19 (2017): 22646.

15. Gupta, S., I.Z. Hlova, T. Kobayashi, R.V. Denys, F. Chen, I.Y. Zavaliy, M. Pruski, and V.K. Pecharsky. "Facile synthesis and regeneration of $Mg(BH_4)_2$ by high energy reactive ball milling of MgB_2." *Chem. Commun*. 49 (2013): 828-830.

16. Pistidda, C., S. Garroni, F. Dolci, E.G. Bardají, A. Khandelwal, P. Nolis, M. Dornheim *et al*. "Synthesis of amorphous $Mg(BH_4)_2$ from MgB_2 and H_2 at room temperature." *J. Alloys Compd.* 508 (2010): 212-215.

17. Li, H.-W., Y. Yan, S. Orimo, A. Züttel, and C.M. Jensen. "Recent progress in metal borohydrides for hydrogen storage." *Energies* 4 (2011): 185-214.

18. Voskuilen, T. G., and T. L. Pourpoint. "Phase field modeling of hydrogen transport and reaction in metal hydrides." *Int. J. Hydrogen Energy* 38 (2013): 7363-7375.

19. Yu, H.-C., F. Wang, G. G. Amatucci, and K. Thornton. "A phase-field model and simulation of kinetically asymmetric ternary conversion-reconversion transformation in battery electrodes." *J. Phase Equil. Diff.* 37 (2016): 86-89.